JURNAL KIMIA VALENSI
p-ISSN: 2460-6065; e-ISSN: 2548-3013
Journal homepage: https://journal.uinjkt.ac.id/index.php/valensi
Research Article

Modification of Coal Fly Ash Waste into Manganese-Oxide-Coated-Zeolite (MOCZ) to Adsorb Heavy Metal Ions Ni^{2+}

Sulistyo Saputro*, Lina Mahardiani, Endang Susilowati, Nanik Dwi Nurhayati, Wirawan Ciptonugroho, Ananda Dea Windiasty, Alita Selvi Prihantoro

Chemistry Education, Sebelas Maret University, Surakarta, Central Java, 57126, Indonesia

Email: sulistyo_s@staff.uns.ac.id

Article Info
Received: Nov 11, 2023
Revised: March 01, 2024
Accepted: May 01, 2024
Online: June 11, 2024

Citation:
Saputro, S., Mahardiani, L., Susilowati, E., Nurhayati, N. D., Ciptonugroho, W., Windiasty, A. D., & Prihantoro, A. S. (2024). Modification of Coal Fly Ash Waste into Manganese-Oxide-Coated-Zeolite (MOCZ) to Adsorb Heavy Metal Ions Ni^{2+}. *Jurnal Kimia Valensi*, *10*(1), 133 – 144.

Doi: 10.15408/jkv.v10i1.35794

Abstract

High consumption of coal as a source of electrical energy in Indonesia has resulted in piles of waste from coal burning, namely fly ash, which can damage the environment and harm health. Fly ash contains main oxides, namely silica (SiO_2) and alumina (Al_2O_3), whose components are similar to zeolite, so they can be synthesized into zeolite-like material (ZLM) which can be used as an adsorbent for heavy metal Ni^{2+}. Therefore, this research discussed the characterization of manganese-oxide-coated-zeolite (MOCZ) from fly ash waste as a heavy metal adsorbent. The research procedure consisted of preparation, purification, and activation stage of fly ash to obtain fly ash that is free from impurities, the stage of making sodium silicate and sodium aluminate, and zeolite synthesis. The resulting zeolite was then coated with manganese oxide to expand the surface area of the zeolite and increase the ability of zeolite to adsorb heavy metal Ni^{2+}. The research results showed that fly ash waste that was coated with manganese oxide can adsorb heavy metal Ni^{2+}. The adsorption of the Ni^{2+} metal ion solution by zeolite with MOCZ modification is in line with the pseudo-second-order kinetic and Langmuir isotherm.

Keywords: MOCZ; fly ash; heavy metal Ni^{2+}

1. INTRODUCTION

Indonesian industries have grown rapidly from year to year as shown by the increasing number of industrial sectors emerging such as textiles, paper, food processing, and other industries. The acceleration of industrial growth causes not only positive impacts but also negative impacts resulting from industrial processes, such as environmental pollution by heavy metal ion pollution. One of the heavy metals produced from this industrial process is nickel (Ni). Some industries produce waste that has a high nickel content, so it is necessary to treat the waste first before it can be discharged into the waters. One of the metal plating enterprises that produces liquid waste from the heavy metal Ni to water is PT. Wahana Kreasi Produk Kencana (PT WKHK) Tangerang[1]. A study conducted by Wibowo et al. (2020) revealed that the levels of Ni metal around Kendari Bay which were analyzed using AAS instrumentation showed high levels of Ni metal. The levels of Ni metal at five locations, namely (T1) Pelabuhan Perikanan Samudera (T2) Wisata Agribisnis Kendari (T3) Masjid Al-Alam (T4) Kendari Beach (T5) Pelabuhan Nusantara Kendari selected based on the number of community activities, varied, respectively TI<T4<T3<T2<T5, namely 0.047 mg/L; 0.052 mg/L; 0.063 mg/L; 0.068 mg/L; 0.073 mg/L[2]. Based on quality standards, the Ni content in seawater is 0.05 mg/L referring to the Minister of Environment Decree (MED) regulations so the levels of Ni metal of T2, T3, T4, and T5 have exceeded the threshold. This is due to high community activity so the value of Ni metal from waste disposal increases. When nickel compounds enter the food chain, these compounds can cause humans and animals to experience consistent nickel accumulation. Ni^{2+} is a toxic waste found in electroplating, zinc base castings, and storage battery parts. Higher concentrations of nickel can cause bone, nose, and lung cancer. One of the most common side effects is dermatitis, such as using coins and jewelry. Acute Ni^{2+} poisoning causes headache, nausea, shortness

of breath, dry cough, nausea, chest pressure, rapid breathing, cyanosis, and extreme fatigue [2].

Other problems arise from coal production processes as a source of electrical energy. This also raises other problems because fly ash waste is still underutilized and poses an environmental hazard if it is carried into waters or blown by strong winds. According to the data from the Ministry of Energy and Mineral Resources (2021), the amount of coal consumed in 2021 reached 113 million tons which was used in the power generation sector, giving rise to piles of coal waste in the form of fly ash and bottom ash which are estimated at 11.3 million tons. in 2021. The fly ash waste produced from coal combustion remains underutilized and is simply piled up in industrial areas, resulting in stockpiling which can damage the environment if it is carried into waters. In addition, it is also dangerous for the surroundings and can interfere with breathing if the fly ash is blown away by strong winds because fly ash contains high levels of metal oxides.

Fly ash contains 42.7% of silica (SiO_2), 22.33% of alumina (Al_2O_3), and 12.41% of iron oxide (Fe_2O_3). High levels of silica and alumina components can be used as zeolites by synthesizing them into materials that have zeolite-like components or Zeolite Like Material (ZLM) [3]. Zeolite has a porous structure that can be used as an adsorbent material for aquatic heavy metals because it has a high cation exchange capacity and surface absorption properties [43]. Adsorptivity of synthetic zeolite from fly ash as an adsorbent can absorb 99.04% of lead metal (Pb) (Ramadani et al., 2017)). The absorption efficiency of zeolite adsorbents on Cr metal is 91.22% (Sobah et al., 2021). However, the presence of impurities in the zeolite structure and its nature which is not optimized by nature causes the zeolite to have a low adsorption capacity [7]. Therefore, modifications are needed to increase the adsorption capacity of zeolite against heavy metals. This modification aims to remove impurities that block fly ash pores so that its absorption capacity increases. One method that can be used to modify zeolite is by coating metal oxide on the zeolite to increase the efficiency of metal removal by the zeolite.[8] The metal oxide coating chosen to modify the zeolite in this research is manganese oxide coating or manganese-oxide-coated-zeolite (MOCZ).

MOCZ is a modified form where zeolite acts as a manganese oxide support. MOCZ has been used as an adsorbent for various heavy metal ions such as Zn^{2+}, Cd^{2+}, and Cu^{2+} [9]. The surface morphology of zeolite changes after chemical treatment with manganese oxide. Manganese oxide has a high ability to reduce aquatic heavy metals through a high oxidation capacity and a coprecipitation process that can be used as a zeolite modification[4]. Zeolite coated with manganese oxide has a good ability to absorb metal ions in water, namely 80%[5]. The absorption of metal ions is better in the zeolite adsorbent coated with manganese oxide, namely 51.1394% than the zeolite adsorbent which can absorb metal ions by 47.6074%.[12] Based on this background, it is necessary to carry out research regarding the coating of manganese oxide on synthetic zeolite from fly ash to overcome the problem of heavy metal Ni pollution, as well as overcome the problem of residual coal production so it does not endanger the environment and the health of the surrounding community.

2. RESEARCH METHOD

The equipment used in this study included glassware, erlenmeyer, glass funnels, dropper pipette, micropipette, spatula, watch glass, measuring flasks, stirrer, desiccator, 100 mesh sieve, furnace, electric heater, magnetic stirrer, autoclave, oven, Buchner funnel, thermometer, stopwatch, digital balance, Whatman paper No.42, and universal pH indicator. Some of the materials used were fly ash, distilled water, HCl 5M from HCl 37%, NaOH 6M, $Al(OH)_3$, $MnCl_2$ 0,1M, $KMnO_4$ 0,1M, $FeCl_3.6H_2O$, and HNO_3 65%. The instrumentations used were a set of FTIR (Fourier Transform Infrared Spectrophotometry) equipment from Shimadzu, a set of XRF (X-Ray Fluorescence) equipment, a set of XRD (X-Ray Diffraction) equipment from Bruker D2 Phaser, and a set of AAS (Atomic Absorption Spectrophotometry) equipment from The Thermo Scientific iCE 3000 AA05202804 v1,30.

2.1 Preparation and Activation of Fly Ash

The preparation stage was carried out by modifying the previous research [6-8]. The steps taken were to take 100 grams of fly ash and then wash it with distilled water. Next, the fly ash was dried in a desiccator and oven at 100 °C for 3 h. The fly ash obtained was then sieved using a 100-mesh sieve to uniformize the size and characterized using XRF, XRD, and FTIR. Then, the fly ash was activated in a furnace at a temperature of 600 °C for 2 h. After the sample was cooled, mix 60 g of fly ash with 200 mL of 5 M HCl for 4 hours. Then, the fly ash was rinsed with distilled water until the pH was neutral, then filtered and dried in an oven at 105 °C for 8 hours. Characterizing was done by activating fly ash using XRD and FTIR.

2.2 Synthesis of Sodium Silicate and Sodium Aluminate

The prepared fly ash was then dissolved in 5 g in 50 mL of 6M NaOH and then heated at 90 °C for 2 h. In the process of making sodium aluminate, 30 g of NaOH was dissolved in 250 mL of distilled water and heated. Then, 17 g of $Al(OH)_3$ was added to the NaOH solution slowly while stirring until completely dissolved and sodium aluminate was finally formed.

2.3 Synthesis of Zeolite

The zeolite synthesis process was carried out by adding sodium aluminate solution slowly to the sodium silicate solution. Then the mixture was stirred for 4 hours until a white gel was produced. The gel formed was then put into an autoclave for 4 h at a temperature of 160 °C. Then, the obtained solid was filtered and dried in the oven for 2 h at a temperature of 105 °C. The resulting zeolite was then characterized using XRF to determine the content of metal compounds or oxides contained in fly ash and to analyze the chemical composition and concentration of elements contained in fly ash. After that, the resulting zeolite was then characterized using XRD to determine the type and mineral content and was carried out using a Philips Xpert MPD XRD diffractometer with operating conditions of 30 mA 40.0 Kv in the 2θ range (5°-90°) and FTIR to determine its functional groups using the KBr pellet method in the infrared spectrum with a wave number of 4000-400 cm^{-1}.

2.4 The process of Manganese-Oxide-Coated-Zeolite

Manganese oxide coating on zeolite was carried out by washing the zeolite with distilled water, then filtering and drying it for 1 hour in an oven at 70 °C. Then 20 g of the prepared zeolite was mixed with 300 mL of 0.1M $MnCl_2$ solution and stirred for 5 h at 25 °C. Next, the zeolite was washed with deionized water, then it was filtered and dried for 1 hour in an oven at 70 °C. Then 10 g of the powder obtained was added with 100 mL of 0.1M $KMnO_4$ solution and stirred for 1 h. The zeolite that had been coated with MnO_2 was then washed with deionized water, then filtered, and dried for 1 h in an oven at 70 °C.

2.5 Adsorbent Characterization

The modified adsorbent was then characterized using XRD, XRF, FTIR, and AAS. XRD instruments were used to determine the type and mineral content found in zeolites. XRF was used to analyze elements in materials qualitatively and quantitatively. FTIR was used to determine the functional groups of adsorbents. AAS was used to determine the adsorption capacity that can be absorbed by adsorbents against heavy metals as pollutants.

2.6 Adsorption of Ni^{2+} Heavy Metal Ions by MOCZ Modified Zeolite

A total of 15 mL of 10 ppm Ni^{2+}metal ion solution was put into 5 250 mL Erlenmeyer flasks. Then 0.4 grams of MOCZ modified zeolite was added. After that, the mixture was separated using a shaker at a speed of 100 rpm and time variations of 30, 60, 90, 120, 150, 180, and 240 minutes respectively. The solution was filtered and the filtrate was taken to measure the absorbance with AAS.

2.7 Calculation of Crystal Size and Crystallinity

$$\text{Crystal size (D)} = \frac{K\lambda}{\beta \cos \theta}$$

Information:
D = crystal size
K = shape factor of the crystal (0.9-1)
λ = wavelength of X-rays (1.5406 Å)
β = value of Full Width at Half Maximum (FWHM) (rad)
θ = diffraction angle (degrees)

$$\text{Crystallinity} = \frac{\text{Crystal area fraction}}{\text{Crystal area fraction} + \text{Amorphous area fraction}}$$

Information:
Crystal area fraction = B crystal × intensity
Amorphous area fraction = B amorphous × intensity
β = ½ ($2\theta_2$ - $2\theta_1$)

3. RESULTS AND DISCUSSION

3.1 Preparation and activation of Fly Ash

In this research, the activation process was carried out using two methods, namely physical and chemical activation. Physical activation was carried out using the hydrothermal method with a temperature variation of 600 °C with a holding time of 2 h. The hydrothermal process was done by inserting a mixture of activated carbon that was still rich in air into a crucible and heating it in a furnace. This activation was carried out to ensure that the air and impurities trapped in the fly ash pores evaporate. This resulted in purer fly ash and the remaining carbon attached to the fly ash was also burned.[14]. The physical state of fly ash was brownish after the activation process as shown in Figure 1.

The chemical activation process of fly ash was done using a strong acid solution, namely HCl, to open the pores by dissolving the solids (organic substances or certain metal compounds) that closed the pores. Chemical activation aimed to open the pores of fly ash. This depended on the concentration of the activator substance 15. The higher the activator concentration, the more impurities in the form of organic and inorganic substances dissolved and escaped from the surface of the carbon pores, thereby causing an increase in absorption capacity. After being activated for 4 hours, more metal impurities were oxidized. The yellow color indicated that oxidation occurred and that there were impurity metals dissolved in HCl.

(a) (b) (c)

Figure 1. Differences in results (a) Fly Ash before treatment (b) Fly Ash preparation (c) Fly Ash activation

HCl solvent is an acid that is very effective in reducing impurities contained in solid waste and can liberate metal compounds[3]. The use of HCl can reduce the concentration of iron oxide and alkaline oxides in fly ash. The reaction is as follows:

$$Fe_2O_{3\,(s)} + 6HCl_{\,(aq)} \rightarrow 2FeCl_{3\,(aq)} + 3H_2O_{\,(l)}$$
$$Al_2O_{3\,(s)} + 6HCl_{\,(aq)} \rightarrow 2AlCl_{3\,(aq)} + 3H_2O_{\,(l)}$$

In the activation process, a reaction occurs between the oxide compounds contained in fly ash and HCl to produce $AlCl_3$ and $FeCl_3$. This is because the Cl^- ion has high electronegativity so this ion easily bonds with cations with large valence such as Si^{4+} and Al^{3+}. Cl^- ions can bond more easily with Al ions because the electronegativity value of the Al ion is smaller than the electronegativity of the Si atom. The fly ash was then washed with distilled water until it was in a neutral state. The purpose of washing the fly ash with distilled water was to free Cl ions in the fly ash framework and remove organic impurities attached to the surface of the fly ash [17].

3.2 Synthesis of Zeolite

Zeolite synthesis began with making sodium silicate and making sodium aluminate. This sodium silicate is the main source of silica which is used for zeolite synthesis in the next stage. The reaction that occurs is as follows:

$$SiO_{2\,(s)} + 2NaOH_{\,(l)} \rightarrow Na_2SiO_{3\,(l)} + H_2O_{\,(l)}$$

Sodium aluminate is the main source of aluminum which is used for zeolite synthesis in the next stage. The reaction that occurs is as follows:

$$Al(OH)_{3\,(s)} + 2NaOH_{\,(l)} \rightarrow Na_2Al(OH)_{4\,(l)}$$

The sodium aluminate solution and sodium silicate solution were mixed and stirred for 4 hours until they became homogeneous and formed a white gel (slurry). In alkaline conditions, meaning with a pH > 12, Si ions formed in $Si_4O_8(OH)_4^{4-}$ and $Al(OH)_4^-$. These formed silica and alumina polymers, where these ions were elements that formed a zeolite[42].

The mixing results of sodium silicate and sodium aluminum produced a white gel. Zeolite synthesis was produced by reacting sodium silicate and sodium aluminate. The NaOH used in zeolite synthesis not only functioned as a reagent but also as a metalizer (supporting material) and as a mineralizer. [18]. Mineralizers are used to speed up the crystallization process by increasing its dissolving ability [19]. Apart from that, the use of NaOH in the synthesis of zeolites also functioned as an activator during the melting process to form water-soluble silicate and aluminate salts, which then played a role in the formation of zeolites during the hydrothermal process. [20]. Na^+ cations also played an important role in zeolite formation. Na^+ ions can stabilize the units forming the zeolite framework and are usually required for zeolite formation under hydrothermal conditions. The results of zeolite synthesis are shown in Figure 2. The reactions that occur during melting are as follows: [21]

$$NaOH_{\,(aq)} + Al_2O_3.SiO_{2\,(aq)} \rightarrow Na_2SiO_{3\,(aq)} + NaAl(OH)_{4\,(aq)}$$

Figure 2. Zeolite Fly Ash from the Synthesis Process

The zeolite synthesis process was carried out using the hydrothermal method to cause the crystallization process and uniformize the crystal size. Crystallization in this synthesis process occurred in the transition process from the sol phase to the gel phase. At the crystal formation stage, the amorphous gel underwent a rearrangement of its structure which broke down to form a more regular arrangement with heating, so that an embryonic crystal nucleus can form. The general zeolite formation reaction is as follows:

$Na_2SiO_{3\,(aq)} + Na_2Al(OH)_{4\,(aq)} \rightarrow$

$Na_x[(AlO_2)_y(SiO)_z].hH_2O_{\,(kristal)}$

(Zhely, 2012)

3.3 Characterization Results

3.3.1 FTIR

Fly ash preparation activated with HCl showed an absorption band at a wavelength of 3446.94 cm^{-1} shifted to 3419.94 cm^{-1} which was the stretching vibration of the O-H bond from Si–OH (silanol) caused by H_2O molecules adsorbed on the silica surface [22]. In this case, the addition of HCl to activated fly ash caused a decrease in the transmittance intensity in the FTIR spectra because the acid could damage the structure of the –OH group so that the bound water molecules were released. [23] Then, the fly ash preparation showed an absorption band at wave number 2923.25 cm^{-1} which was the C–H stretching vibration [24]. This showed that fly ash still contained impurities, namely carbon bonds. Meanwhile, in activated fly ash there was an absorption band at wave number 2924.21 cm^{-1} which indicated the bending vibration of the -OH group from Si-OH. This showed that activation with HCl was effective in dissolving impurities in the form of C or carbon atoms and other impurities [25]. Furthermore, in the fly ash preparation, there was a C-H bending vibration at a wave number of 1419.67 cm^{-1}. Then, in prepared fly ash there was a wave number of 1109.12 cm^{-1}, and for activated fly ash there was a wave number of 1065.72 cm^{-1}, namely the presence of asymmetric stretching vibrations of the siloxyl group (≡Si–O) of siloxane (≡Si–O– Si≡). This showed that the crystallinity in the fly ash structure decreased. Then in activated fly ash, there was T-O symmetry stretching vibration of Si-O-Si and Al-O-Si at a wave number of 691.51 cm^{-1}. In the prepared fly ash there were wave numbers of 435.93 cm^{-1} and 420.5 cm^{-1} indicating the presence of T–O bending vibrations from T=Fe or Al which indicated the presence of pore structure and Fe impurities in the fly ash. Then, in activated fly ash there were wave numbers of 449.43 cm^{-1} and 421.46 cm^{-1} which indicated the presence of weak siloxyl group bonds (≡Si–O). This indicated that HCl activation could weaken the interaction of siloxyl groups (≡Si–O) with impurities in the fly ash pores so that the fly ash pores became cleaner and were reinforced by the disappearance of the absorption band at the wave number 1419.67 cm^{-1}.

In the synthesized zeolite, there was absorption at wave numbers 3636.94 and 3425.72 cm^{-1} indicating the presence of -OH groups from Si-OH or water molecules. The -OH group of Si-OH appeared at wave numbers 3019.69 and 2470.92 cm^{-1} which indicated the existence of asymmetric stretching vibrations -OH of Si-OH. Meanwhile, the -OH group from Si-OH was also proven by the absorption wave numbers of 1640.53 and 1446.67 cm^{-1}, which showed that there was a -OH bending vibration from Si-OH. The appearance of spectra at around 3019.69 cm^{-1} and 1640.53 cm^{-1}, which showed stretching vibrations and bending vibrations of water molecules in zeolite, was evidence of the formation of zeolite through an alkaline hydrothermal process [26].

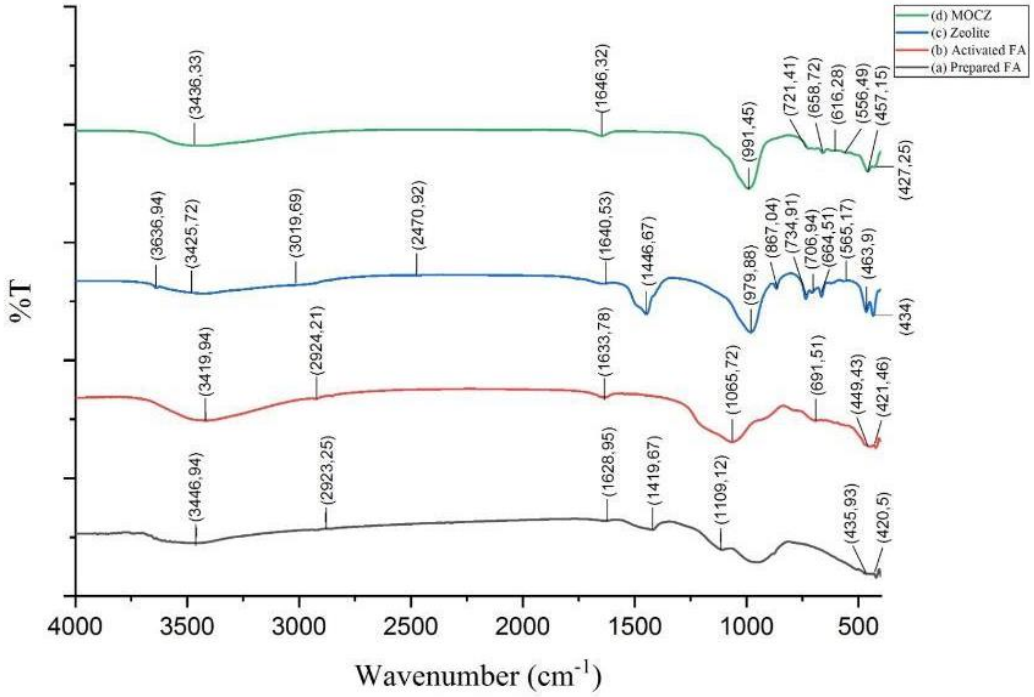

Figure 3. The FTIR of Prepared Fly Ash, Activated Fly Ash, Zeolite, and MOCZ

At lower frequencies, there was an absorption band due to symmetric stretching vibrations of O-Si-O or O-Al-O in the main building frame of the SiO_4 and AlO_4 tetrahedral at wave numbers 664.51 – 867.04 cm^{-1}. One of the characteristics of zeolite is that it is composed of an interconnecting framework of 4 double rings (D4R) which appears in the wave number range 600 – 550 cm^{-1}. The result of the absorption wave number 565.17 cm^{-1} is an indication of the existence of a double ring which is a characteristic of the crystal structure zeolite A[27]. The absorption wave numbers 463.9 and 434 indicated the presence of symmetrical bending vibrations of Si-O-Al.

In the zeolite coated with manganese oxide, there was an absorption at wave number 3436.33 which indicated the presence of O-H stretching and bending vibrations in the manganese oxide structure. The absorption band at 3200-1600 cm^{-1} showed the presence of bending vibrations which indicated the presence of -OH groups from Si-OH or water molecules. In zeolite with MOCZ modification, absorption appeared at wave numbers 991.45 cm^{-1} and 556.49 -658.72 cm^{-1}, respectively, indicating the existence of asymmetric Si-O-Si bending and stretching vibrations in SiO_2 tetrahedra after coating with MnO and Mn-O vibrations of MnO6-octahedral on MnO2 on the zeolite surface [28]. The absorption power appearing at wave numbers 427.25–457.15 cm^{-1} indicated the existence of bending and stretching vibrations of the O-Mn-O bond. The spectrum and analysis results indicated that the zeolite coating using manganese oxide was successful.

3.3.2 XRF

In this research, XRF analysis was carried out for the chemical oxide composition of fly ash, zeolite, and MOCZ which is shown in Table 1, and the chemical element composition of fly ash, zeolite, and MOCZ which is shown in Table 2.

According to the data in the American National Standards published by American Standard Testing and Material (ASTM) C618, fly ash is classified into three classes based on differences in chemical composition, namely type C fly ash, type F fly ash, and type N fly ash. This class has minimum requirements for SiO_2, Al_2O_3, Fe_2O_3, and CaO. In type C fly ash (minimum 50% SiO_2, Al_2O_3, and Fe_2O_3), type F fly ash (minimum 70% SiO_2, Al_2O_3, and Fe_2O_3), and type N fly ash (minimum 70% SiO_2, Al_2O_3, and Fe_2O_3). Table 1 shows that PLTU Adipala fly ash is classified as type C, namely fly ash containing more than 10% CaO and with a total content of SiO_2, Al_2O_3, and Fe_2O_3 less than 70%, namely 13% each; 3.8%; and 39.3%. Type C class fly ash is produced

Table 1. Composition of the Chemical Oxide content of Fly Ash, Zeolite, and MOCZ

Oxide	Fly Ash (%mass)	Zeolite (%mass)	MOCZ (% mass)
SiO_2	13	60.5	24.6
Al_2O_3	3.8	29	16
Fe_2O_3	39.3	0.13	-
CaO	37.3	1.3	-
K_2O	1.1	-	-
TiO_2	1.1	-	-
SO_3	2.2	6	1.4
P_2O_5	0.5	2.8	0.73
MnO	0.49	-	45.97
SrO	0.661	-	-
ZrO_2	0.064	0.04	0.03
BaO	0.32	-	-

Table 2. Composition of the Chemical Element content of Fly Ash, Zeolite, and MOCZ

Element	Fly Ash (%mass)	Zeolite (%mass)	MOCZ (% mass)
Si	8.4	60.9	15.6
Al	2.6	25	11
Fe	44.1	0.29	-
Ca	38.7	2.8	-
K	1.3	-	-
Ti	1	-	-
S	1.2	6.4	0.77
P	0.3	3.4	0.49
Mn	0.59	-	57.82
Sr	0.941	-	-
Zr	0.071	0.1	0.04
Ba	0.46	-	-

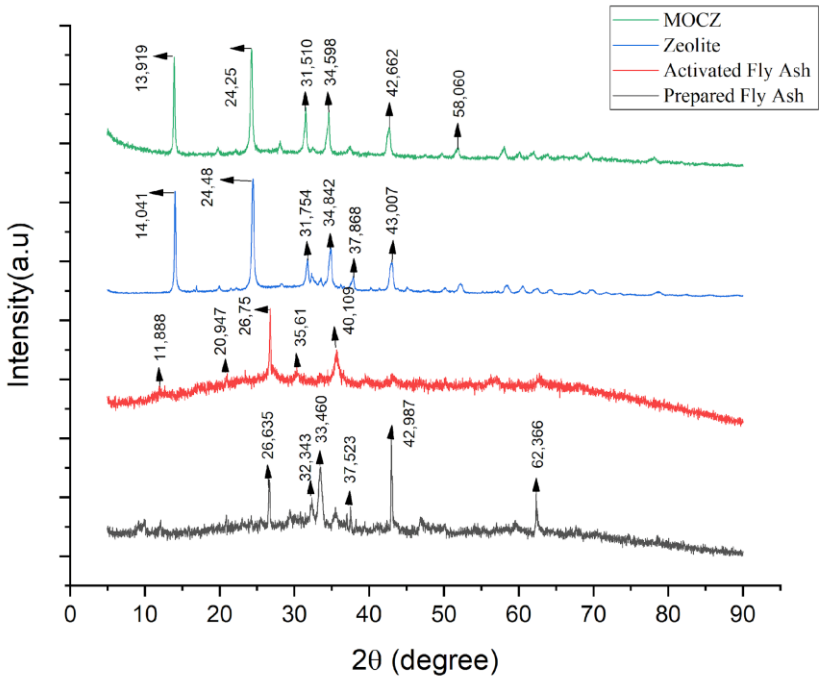

Figure 4. XRD spectrum

from burning lignite and subbituminious coal, and is pozzolanic (it contains silica and alumina compounds) and cementitious. Based on the XRF results, it is known that the SiO_2 and Al_2O_3 content in fly ash is quite large allowing fly ash to be used as an adsorbent. The high levels of these two components in fly ash mean that many active centers on the surface of the solid can interact with adsorbate, for example, metal ions. [29].

Based on the XRF results in Table 1, it can be seen that the SiO_2 content increased from 13% to 60.5%. This is due to the activation treatment with HCl on fly ash so that the metal impurities contained in fly ash are reduced. This is in line with the previous research stating that when fly ash is activated with an acid solution (HCl), the Si-O bonds on the surface increase due to the dissolution of impurities[9]. In addition, HCl solution can reduce the CaO and Fe_2O_3 content in fly ash.

Table 1 shows that the SiO_2 content decreased from 60.5% to 24.6%, which indicates that the fly ash structure was destroyed. Apart from that, after coating with manganese oxide on the zeolite, it was seen that the MnO content increased, from 0% to 45.97%. This means that manganese oxide was successfully synthesized and coated the fly ash [32].

3.3.3 XRD

The diffractogram spectrum in Figure 4 shows that the highest intensity for fly ash appearing at an angle of 2θ = 26.63° was quartz (SiO_2) based on JCPDS No. 88-2302. Meanwhile, angles 2θ = 37.52° and 42.98° were the peaks for mullite which was formed from two components, namely alumina and silica. [33]. The X-ray diffraction pattern of quartz and mullite material in fly ash showed the presence of Si and Al elements[8]. The XRD data in Figure 3 showed that the mineral composition of fly ash changed in the diffractogram before and after activation. This was indicated by the disappearance of the peaks for mullite, namely at angles 2θ = 37.52° and 42.98°. Based on [34] the chemical and physical properties of zeolite and aluminum in fly ash were activated under high temperatures, which converted the crystalline mullite phase into amorphous aluminosilicate.

Figure 4 shows a comparison of the XRD results of fly ash with 5M activated fly ash, showing that there was no significant difference in the peak shape produced. The diffractogram of fly ash and 5M activated fly ash showed the presence of 2 peaks at angles 2θ respectively, namely = 20.94° and 26.63°. These two peaks were peaks for the mineral quartz or SiO_2 based on JCPDS No. 88-2302. In non-modified zeolite, MOCZ showed that the highest intensity appeared at an angle of 2θ = 24.48°, which was the peak for quartz or SiO_2 minerals based on JCPDS No. 88-2302 [35]. The diffractogram of the synthesized zeolite showed a peak at an angle of 2θ = 14.04°; 24.48°; 34.84°; and 43.00° which was the typical peak of zeolite-A.[36]

The X-ray diffraction spectrum contained peaks at 2θ = 13.91 and 24.25 which indicated the presence of mordenite ($Al_2Si_{10}O_{24}.7H_2O$). The peaks 2θ = 31.51 and 34.59 showed the presence of a clinoptilolite (Si, Al)$_{36}O_{72}.20H_2O$ peak. Furthermore, the oxide coating on the zeolite surface, namely vernadite (dMnO2), was at the peak of 2θ = 42.66 [10]. This showed δ-MnO2 with

significant deviation due to Mn-O and Si-O interactions. This peak identified that the manganese oxide formed on the sand surface was the δ-MnO2 polymorph (Chaudhry et al., 2016). Based on the results of XRD analysis and calculations, the crystal size and degree of crystallinity were obtained which showed the difference between non-MOCZ-modified zeolite and MOCZ-modified zeolite. These results can be seen in Table 3.

Table 3. Crystallinity analysis of zeolite without MOCZ modification and zeolite with MOCZ modification

Samples	Crystal size (nm)	Crystallinity (%)
Zeolite	17.959	46
MOCZ	15.574	28

Table 3 shows that the crystal sizes in the prepared fly ash, activated fly ash, zeolite, and MOCZ samples were 17.3983; 18.1614; 17,959; and 15,574 nm. The crystal size affected the adsorption capacity. The smaller the crystal size, the greater the surface area of the pores and constituent parts of the zeolite. The smallest crystal size was in MOCZ, so the surface area of MOCZ was larger. As the crystallinity increased, the crystal size gradually became smaller, so the surface area increased regularly as the crystal morphology changed. This can be attributed to the greater number of micropores that can be accessed at smaller crystal sizes (Luogang Wu, 2021). Thus, this large surface area is effective for use as a heavy metal adsorbent.

The degree of crystallinity of fly ash increased after being activated by acid (HCl), namely from 13% to 13.5%. This is because the acid activation process can increase crystallinity, acidity, and surface area. Activation with acid can increase the purity of silica and reduce impurities in fly ash. Therefore, acid treatment can reduce the aluminum content of the fly ash framework and can increase the acidity of the fly ash [38]. Apart from that, the increase in the degree of crystallinity is also caused by an increase in temperature which causes the intensity of the crystalline phase to increase and the amorphous phase to decrease. This shows an increase in the crystallinity of hydrothermal products due to increasing temperature [39].

The degree of crystallinity of MOCZ-modified zeolite was smaller than the degree of crystallinity of non-MOCZ-modified zeolite. The degree of crystallinity decreased after being modified with manganese oxide due to the tendency of manganese oxide to have amorphous properties which caused the degree of crystallinity to decrease[10]. In addition, reducing the degree of SiO_2 crystallinity can reduce metal levels in waste samples even more. This is because the silica reacted and dissolved in Mn2+, thus forming an amorphous phase. This is in line with research where MOCZ has a low level of crystallinity, the zeolite surface sites are occupied by manganese oxide formed during the coating process and result in a greater adsorption capacity. [10]. This is proportional to the open surface fraction of the adsorbent. In this case, zeolite with an amorphous phase (low degree of crystallinity) is more effective as an adsorbent.[19]

3.4 Contact Time and Kinetic Model

The adsorbent and adsorbate were contacted with adsorbent contact times of 60, 90, 120, 150, 180, and 240 minutes. The research results showed that the ability of zeolite with MOCZ modification to adsorb Ni^{2+} metal ions with variations in contact time was seen at the 180th minute, the adsorption capacity was 0.369 mg/g. This shows that this time is the optimum contact time for the modified zeolite which can absorb Ni^{2+} metal ions maximally. After 180 minutes, there was a decrease in adsorption capacity because most of the adsorbent active sites had bound Ni^{2+} metal ions so changing time does not change the adsorption capacity to be greater. The achievement of the optimum time indicated that the interaction between the metal ions and the active sites of the adsorbent reached equilibrium.[40]

Because the main target is a metal in the form of an ion (cation), the interaction is specific to the interaction between charges[10]. The attachment of metal ions to a charged adsorbent has a specific interaction caused by charge attraction. When an adsorbent has been activated, metal ions attach to the adsorbent so that the cations are bound to the active site which has a negative charge due to charge attraction interactions. Adsorption occurs electrostatically and deprotonates the hydroxyl surface from the oxide support site which contains active ions. Cations are absorbed on the surface of the adsorbent support or the diffusion part of the double layer.

Table 4. Contact time MOCZ on the adsorption of Ni^{2+} metal ions

Time (minutes)	(C_0) (mg/L)	(C_e) (mg/L)	(Q) (mg/g)	(adsorption efficiency) (%)
30	10.0891	5.3426	0.177	47.04
60	10.0891	4.6579	0.203	53.8
90	10.0891	2.7606	0.207	72.6
120	10.0891	1.3729	0.326	86.3
150	10.0891	0.7357	0350	92.7
180	10.0891	0.2465	0.369	97.5
240	10.0891	1.0669	0.338	89.4

Table 5. Ni^{2+} metal ion adsorption kinetic model

Kinetic Models	Equation	R^2	k (minute^{-1})	C_0 (mg/L)	Q_e (mg/g)
First order	y = -0.0118x + 1.8866	0.6144	0.0118	6.5969	-
Second order	y = 0.0071x + 0.1187	0.1292	0.0071	8.4245	-
Pseudo 1	y = -0.0045x - 1.7991	0.0566	0.0045	-	0.1654
Pseudo 2	y = 2.315x + 109.83	0.9599	0.0488	-	0.4319

Table 4 shows that there was an increase in adsorption efficiency from an initial time of 0 minutes to optimum absorption up to a contact time of 180 minutes and then decreased at 240 minutes. At a contact time of up to 180 minutes, the number of Ni^{2+} metal ions adsorbed increased and reached optimum at a contact time of 180 minutes. This happened because the longer the interaction time between the adsorbent and Ni^{2+} metal ions, the more collisions that occur, the more Ni^{2+} metal ions can be adsorbed. At a contact time of less than 180 minutes, the active site was not filled with Ni^{2+} metal ions so that the Ni^{2+} metal ions could be adsorbed quickly and after a contact time of 180 minutes, the graph tended to decrease until 240 minutes. The decrease in adsorption of Ni^{2+} metal ions was indicated due to desorption or release from the adsorbent which was caused by the weak interaction that occurred between Ni^{2+} metal ions and the adsorbent to bind to the surface of the adsorbent. The optimum contact time was achieved at 180 minutes with an adsorption percentage of 97.5%. This phenomenon occurred when the optimum contact time was reached. The adsorbent experienced too much desorption due to the active sites available on the surface of the adsorbent decreasing because the metal ion solution formed a new layer on the surface of the adsorbent so that it covered the adsorbent layer. So when the optimum contact time was exceeded, the adsorption power decreased.[41]

The reaction kinetic models used in this research are pseudo-order one and pseudo-order two. It can be concluded that the appropriate reaction order for the adsorption of Ni^{2+} metal ion solutions by zeolite with MOCZ modification is pseudo reaction order 2. In Table 4, the linear equations of the pseudo-first-order model and the pseudo-second-order is ln (qe-qt) = -0.0045t - 1.7991 and t/Qt = 2.315t + 109.83 with the correlation coefficient (R^2) in the pseudo-first-order and pseudo-second-order models respectively being 0.0566 and 0, 9599. The results of the data analysis show that the adsorption of the Ni^{2+} metal ion solution by zeolite with MOCZ modification is in line with the pseudo-second-order kinetic model because the correlation coefficient (R^2) value is close to 1. This is in line with research by Irannajad (2017) showing that the zeolite material with modified manganese oxide (MCOZeo) used to adsorb the elements Co^{2+}, Ni^{2+}, and Pb^{2+} follows the Ho & Mc Key adsorption kinetic mechanism or pseudo-second-order kinetics.

3.5 Adsorption Isotherm

The adsorption study shows that the Langmuir adsorption isotherm has an R^2 value of 0.9859, while the Freundlich isotherm adsorption has an R^2 value of 0.8348. Therefore, the results of the data analysis showed that the adsorption of Ni^{2+} metal ions with zeolite with MOCZ modification followed the Langmuir isotherm equation because the correlation coefficient (R^2) value was close to 1. The Ni^{2+} metal ion adsorption isotherm pattern has the equation y = 5.7781x - 2.4719 so it can be seen that the price of a was 0.1730 and b was 2.3384. Determination of Langmuir and Freundlich constant values is based on contact time variation data.

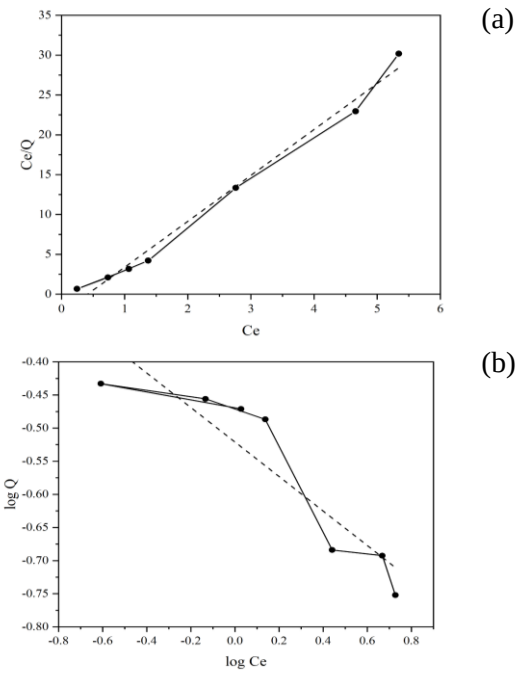

Figure 6. Adsorption isotherm graph (a) Langmuir (b) Freundlich of Ni^{2+} metal ions

Table 6. Adsorption Isotherms

Adsorption Isotherm	Constant	Value (mg/g)
Langmuir	a	0.1730
	b	2.3384
Freundlich	K	6.8359
	n	3.8402

In the process of adsorption of Ni^{2+} ions using MOCZ, when Ni^{2+} ions entered the water, then the adsorption process occurred and there was an interaction

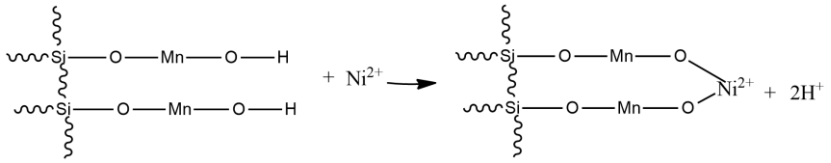

Figure 7. Reaction mechanism of MOCZ with Ni ions

of Ni^{2+} ions bound to MOCZ which was preceded by the release of two hydrogen ions [43]. This caused Ni^{2+} ions to be adsorbed and bound to MOCZ so that their concentration in the water was reduced.

CONCLUSIONS

Based on the discussion, the smaller the crystal size, the larger the surface area of MOCZ which is brown, and its adsorption ability increases, so the results of MOCZ characterization from fly ash waste, as shown by the results of FTIR and XRD characterization, can be used as an adsorbent for the heavy metal Ni^{2+}. This is reinforced by the results of the influence of the contact time of the MOCZ adsorbent on the adsorption efficiency of the heavy metal Ni^{2+}, namely that the longer the contact time of the zeolite with the heavy metal Ni^{2+}, the greater the adsorption efficiency of the heavy metal Ni^{2+} produced.

ACKNOWLEDGEMENTS

The authors would like to express their gratitude to the Institute of Research and Community Services (LPPM) Universitas Sebelas Maret, Surakarta, Indonesia for funding this research through Research Group Grant No. 228/UN27.22/PT.01.03/2023.

REFERENCES

1. Wibowo D, Basri B, Adami A, et al. Analisis Logam Nikel (Ni) dalam Air Laut dan Persebarannya di Perairan Teluk Kendari, Sulawesi Tenggara. *Indo J Chem Res*. 2020;8(2):144-150. doi:10.30598//ijcr.2020.8-dwi
2. Parmar M, Singh Thakur L. Heavy metal Cu, Ni and Zn: Toxicity, health hazards and their removal techniques by low cost adsorbents: A Short overview. *Int J Plant, Anim Environmetal Sci*. 2013;3(3):143-157.
3. Mufrodi Z, Sutrisno B, Hidayat A. Modifikasi Limbah Abu Layang sebagai Material Baru Adsorben. In: *Prosiding Seminar Nasional Teknik Kimia "Kejuangan"* . ; 2010:1-5.
4. Hong M, Yu L, Wang Y, et al. *Heavy Metal Adsorption with Zeolites: The Role of Hierarchical Pore Architecture*. Vol 359. Elsevier B.V.; 2019. doi:10.1016/j.cej.2018.11.087
5. Ramadani K, Kimia J, Sains dan Teknologi F, Alauddin Makassar U, Tinggi Agama Islam Negeri Watampone S. *Sintesis Zeolit Dari Abu Layang (Fly Ash) Dan Uji Adsorptivitas Terhadap Logam Timbal (Pb) Al-Kimia*|. Vol 5.; 2017.
6. Sobah S, Anoi YH, Diana, Octavianus P. Kesetimbangan Adsorpsi Isotermis Logam Cr (VI) pada Fly Ash. *Al Ulum J Sains dan Teknol*. 2021;6(2):39-43.
7. Weitkamp J. Zeolites and Catalysis. *Solid State Ionics*. 2014;2(3):175-188. doi:10.1177/2324709614545225
8. Nouh ESA, Amin M, Gouda M, Abd-Elmagid A. Extraction of uranium(VI) from sulfate leach liquor after iron removal using manganese oxide coated zeolite. *J Environ Chem Eng*. 2015;3(1):523-528. doi:10.1016/j.jece.2015.01.013
9. Irannajad M, Haghighi HK. Removal of Co2+, Ni2+, and Pb2+ by manganese oxide-coated zeolite: Equilibrium, thermodynamics, and kinetics studies. *Clays Clay Miner*. 2017;65(1):52-62. doi:10.1346/CCMN.2016.064049
10. Taffarel SR, Rubio J. Removal of Mn2+ From Aqueous Solution by Manganese Oxide Coated Zeolite. *Miner Eng*. 2010;23(14):1131-1138. doi:10.1016/j.mineng.2010.07.007
11. Khashij M, Mousavi SA, Mehralian M, Massoudinejad MR. Removal of Fe2+ From Aqueous Solution Using Manganese Oxide Coated Zeolite and Iron Oxide Coated Zeolite. *Int J Eng Trans B Appl*. 2016;29(11):1587-1594. doi:10.5829/idosi.ije.2016.29.11b.13
12. Hasan A, Yerizam M, Habib Yahya M, et al. Mekanisme Adsorben Zeolit dan Manganese Zeolit terhadap Logam Besi (Fe). *J Kinet*. 2021;12(01):9-17. https://jurnal.polsri.ac.id/index.php/kimia/index
13. Sunarti, Nazudin. Sintesis Zeolit A dari Abu Dasar Batubara (Coal Bottom Ash) dengan Metode Peleburan dan Hidrotermal. *Molluca J Chem Educ*. 2021;11(1):8-16. doi:10.30598/mjocevol11iss1pp8-16
14. Nurdiansah H, Susanti D. Pengaruh Variasi Temperatur Karbonisasi dan Karbon Aktif Tempurung Kelapa dan Kapasitansi Electric Double Layer Capacitor. *J Tek Pomits*. 2013;2(1):13-18.
15. Gumelar D, Hendrawan Y. Pengaruh Aktivator dan Waktu Kontak Terhadap Kinerja Arang Aktif Berbahan Eceng Gondok (Eichornia crossipes) Pada Penurunan COD Limbah Cair Laundry. *J Keteknikan Pertan Trop dan Biosist*. 2015;3(1):15-23.
16. Sutrisno B, Hidayat A, Mufrodi Z. Modifikasi Limbah Abu Layang menjadi Adsorben untuk Mengurangi Limbah Zat Warna pada Industri Tekstil. *Chem J Tek Kim*. 2016;1(2):57. doi:10.26555/chemica.v1i2.3571
17. Pata A, Sitorus S, Gunawan R. Pemanfaatan abu batubara sebagai zeolit yang terdealuminasi dalam mengadsorpsi fenol. *J Kim Mulawarman*. 2014;12(November):19-24.

18. Deviani SS, Mahatmanti FW, Widiarti N. Indonesian Journal of Chemical Science Sintesis dan Karakterisasi Zeolit dari Abu Sekam Padi Menggunakan Metode Hidrotermal. *Indones J Chem Sci*. 2018;7(1).
19. Jumaeri, Astuti W, W.T.P. Lestari. Preparasi dan Karakterissi Zeolite dari Abu Layang Batubara Secara Alkali Hidrotermal. *Reaktor*. 2007;11(1):38-44.
20. Ojha K, Pradhan NC, Samanta AN. Zeolite from Fly Ash: Synthesis and Characterization. *Bull Mater Sci*. 2004;27(6):555-564. doi:10.1007/BF02707285
21. Andarini N, Lutfia Z, Haryati T. Sintesis Zeolit A dari Abu Terbang (Fly Ash) Batubara Variasi Rasio Molar Si/Al Synthesis of Zeolite A From Coal Fly Ash with Variation of Si/Al Molar Ratio. *J Ilmu Dasar*. 2018;19(2):105-110.
22. Imoisili PE, Jen TC. Synthesis and Characterization of Amorphous Nano Silica From South African Coal Fly Ash. In: *Materials Today: Proceedings*. Elsevier Ltd; 2023:1-6. doi:10.1016/j.matpr.2023.06.077
23. Ghofur A, Atikah, Soemarno, Hadi A. Karateristik Fly Ash Batubara Sebagai Bahan Katalik Konverter dalam Mereduksi Gas Buang HC dan CO Kendaraan Bermotor. In: *Universitas Brawijaya Malang*. ; 2014:33-37.
24. Kanjana N, Maiaugree W, Laokul P, et al. Fly Ash Boosted Electrocatalytic Properties of PEDOT: PSS Counter Electrodes for The Triiodide Reduction in Dye-sensitized Solar Cells. *Sci Rep*. 2023;13(1):1-15. doi:10.1038/s41598-023-33020-6
25. Triviana L, Sugiarti S, Rohaeti E. Sintesis Dan Karakterisasi Natrium Silikat (Na2SiO3) dari Sekam Padi. *J Sains dan Teknol Lingkung*. 2015;7(2):90-97.
26. Mokgehle TMA, Gitari WM, Tavengwa NT. Synthesis and characterization of zeolites produced by ultrasonication of coal fly Ash/NaOH slurry filtrates. *South African J Chem*. 2020;73:64-69. doi:10.17159/0379-4350/2020/V73A10
27. Ren X, Qu R, Liu S, et al. Synthesis of Zeolites From Coal Fly Ash for The Removal of Harmful Gaseous Pollutants: A Review. *Aerosol Air Qual Res*. 2020;20(5):1127-1144. doi:10.4209/aaqr.2019.12.0651
28. Chaudhry SA, Khan TA, Ali I. Adsorptive removal of Pb(II) and Zn(II) from water onto manganese oxide-coated sand: Isotherm, thermodynamic and kinetic studies. *Egypt J Basic Appl Sci*. 2016;3(3):287-300. doi:10.1016/j.ejbas.2016.06.002
29. Sari, Y. A., Saputro, S. H., & Prasetya, A. T. Penentuan Kadar Nikel Dalam Mineral Laterit Dengan Metode Kopresipitasi Menggunakan Cu-Pirolidin Ditiokarbamat. *Indonesian Journal of Chemical Science*, 2013;2(3).
30. Li Y, Zhang FS, Xiu FR. Arsenic (V) Removal from Aqueous System Using Adsorbent Developed From a High Iron-containing Fly Ash. *Sci Total Environ*. 2009;407(21):5780-5786. doi:10.1016/j.scitotenv.2009.07.017
31. Lv Z, Pan X, Geng X, Yu H. Synergistic Removal of Calcium and Iron Impurities from Calcium-rich and High-alumina Fly Ash by Acid Leaching Control. *J Environ Chem Eng*. 2022;10(2):107268. doi:10.1016/j.jece.2022.107268
32. Zhao Y, Wang F, Yang J, et al. Synthesis of Coal Fly Ash-based Heterogeneous Fenton Catalyst for Bisphenol a Removal: Performances and Proposed Mechanism. *Vacuum*. 2023;212(53):112054. doi:10.1016/j.vacuum.2023.112054
33. Sun Q, Zhao S, Zhao X, Song Y, Ban X, Zhang N. Influence of Different Grinding Degrees of Fly Ash on Properties and Reaction Degrees of Geopolymers. *PLoS One*. 2023;18(3):1-25. doi:10.1371/journal.pone.0282927
34. Zhuang XY, Chen L, Komarneni S, et al. Fly Ash-based Geopolymer: Clean Production, Properties and Applications Xiao. *J Clean Prod*. Published online 2016. doi:10.1016/j.jclepro.2016.03.019
35. Amma A, Mahatmanti FW, Widiarti N. Indonesian Journal of Chemical Science Esterifikasi Minyak Jelantah. *J Chem Sci*. 2018;7(3):264-266.
36. Raharjo Y, Fahmi MZ, Wafiroh S, Widati AA. Incorporation of Imprinted-Zeolite To Polyethersulfone/Cellulose Acetate Membrane for Creatinine Removal in Hemodialysis Treatment. *J Teknol (Sciences Eng*. 2019;81(3):137-144. doi:10.11113/jt.v81.13075
37. Chaudhry SA, Khan TA, Ali I. Adsorptive Removal of Pb(II) and Zn(II) from Water Onto Manganese Oxide-coated Sand: Isotherm, Thermodynamic and Kinetic Studies. *Egypt J Basic Appl Sci*. 2016;3(3):287-300. doi:10.1016/j.ejbas.2016.06.002
38. Nurmalita N, Madjid SN, Setiawan A, Idroes R, Jalil Z. Characteristics of Silica Powder Extracted from Fly Ash of Coal Fired Power Plant – Effect of Heat Treatment Process. *J Ecol Eng*. 2023;24(9):282-292. doi:10.12911/22998993/169289
39. Ryu G., Kim G., Khalid HR, Lee H. The Effects of Temperature on the Hydrothermal Synthesis of Hydroxyapatite-Zeolite Using Blast Furnace Slag. *Materials (Basel)*. 2019;12(2131):1-12. doi:10.3390/ma12132131
40. Puspitarini R, Sn AK, Ar R. Effect of Particle Size , Activator Agent , Activation Time and Adsorption Time on the Ability of Fly Ash to Adsorb Cadmium (Cd) from Leachate in the Final Disposal Area (TPA) in Purworejo, Central Java. *J Sains dan Terap Kim*. 2019;13(2):109-118.
41. Aisyahlika SZ, Firdaus ML, Elvia R. Kapasitas Adsorpsi Arang Aktif Cangkang Bintaro (Cerbera odollam) Terhadap Zat Warna Sintesis Reactive RED-120 Dan Reactive BLUE-198. *J Pendidik Dan Ilmu Kim*. 2018;2(2):148-155.
42. Febrianti, R. F., Zaharah, T. A., & Adhitiyawarman. (2022). Sintesis Zeolit A Berbahan Daar Abu Terbang (Fly Ash) Limbah PT. Indonesia Chemical Alumina (ICA) Menggunakan Metode Alkali Hidrotermal. *Indonesian Journal of Pure and Applied Chemistry*, *5*(1), 28–39. http://jurnal.untan.ac.id/index.php/IJoPAC%0ASINTESIS

43. Xu, P., Zeng, G., Huang, D., Lai, C., Zhao, M., & Wei, Z. Et Al. (2012). Adsorption Of Pb(Ii) By Iron Oxide Nanoparticles Immobilized Phanerochaete Chrysosporium: Equilibrium, Kinetic, Thermodynamic And Mechanisms Analysis. *Chemical Engineering Journal*, *203*, 423-431. Https://Doi.Org/10.1016/J.Cej.2012.07.048